LA-UR- 00-1192

Approved for public release; distribution is unlimited.

Title: AN EVALUATION OF SEVERAL HARDENING MODELS USING TAYLOR CYLINDER IMPACT DATA

Author(s): MARVIN A. ZOCHER, X-7, MS D413
PAUL J. MAUDLIN, T-3, MS B216
SHUH RONG CHEN, MST-8, MS G755
ELANE C. FLOWER-MAUDLIN, X-4, MS F664

Submitted to: EUROPEAN CONGRESS ON COMPUATIONAL METHODS IN APPLIED SCIENCES AND ENGINEERING
BARCELONA, SPAIN
SEPTEMBER 11-14, 2000

Los Alamos
NATIONAL LABORATORY

DISCLAIMER

DISCLAIMER

Portions of this document may be illegible in electronic image products. Images are produced from the best available original document.

An Evaluation of Several Hardening Models Using Taylor Cylinder Impact Data

Marvin A. Zocher, Paul J. Maudlin, Shuh Rong Chen, and Elane C. Flower-Maudlin

University of California
Los Alamos National Laboratory
X-7, MS D413
Los Alamos, NM 87545, USA
e-mail: zocher@lanl.gov

Key words: Plasticity, Hardening Model, Taylor Cylinder, Flow Stress

Abstract. *A semi-implicit formulation of rate-independent classical plasticity, as implemented in a three dimensional continuum mechanics code is discussed. The plasticity formulation employs an associative flow rule for the evolution of plastic strain, an anisotropic yield criterion, an application of Nemat-Nasser's semi-implicit method for updating the deviatoric stress, and isotropic hardening through the evolution of a flow stress. Several different hardening rules have been implemented. Preliminary evaluation of these hardening models, based on an ability to predict the results of Taylor cylinder impact, are presented. The evaluation is based on a comparison of predicted final deformed shape to experimentally measured final deformed shape. Test results obtained from experiments conducted using two different copper materials and tantalum are included in the evaluation.*

1 INTRODUCTION

The thermomechanical problem of predicting the behavior of metallic components undergoing large deformation plastic flow is of central importance in a number of applications. Consequently, this is a field of mechanics which has received significant attention over at least the last one hundred-fifty years. Even with such sustained attention, the problem remains one that is not fully resolved. One reason for this is that closed form solutions are almost always untenable, and the computational capabilities necessary to solve the numerical approximation of the physical thermomechanical problem have until recently been beyond the reach of even the most capable computers and numerical techniques. This may still be the case, but capabilities are now becoming available which enable us to advance our understanding of the large deformation problem, at least incrementally.

One aspect of the problem which remains an as yet unresolved issue is a determination of the most appropriate formulation for a model intended to predict hardening. Independent variables that effect hardening behavior certainly include strain, strain rate, and temperature, but perhaps others as well. One factor that complicates the determination of the most appropriate hardening formulation is that these independent variables reside in a domain which can be quite large. Moreover, it may be that a model which works well in one loading regime will fail miserably in another. Consequently, an objective of validating a general purpose hardening model necessarily requires comparing its predictive capabilities in a variety of pertinent loading regimes.

The authors, along with several colleagues, have undertaken the task of assessing the ability of several proposed hardening models to accurately predict hardening over a loading regime that is within the reach of simple experimental validation techniques such as Taylor cylinder impact and plane-strain flyer plate impact. The present work focuses on an evaluation of three proposed models and is based on comparison of prediction to experimental data derived from Taylor cylinder impact. Other loading regimes will be addressed at a later date. The Taylor test is considered a good test for the evaluation of plasticity models because it produces a variety of macroscopically observable material behaviors and rather large gradients in strain, strain rate, and to a lesser degree, temperature. The result is an integrative test which serves to excercise many aspects of the plasticity model in general, and of hardening in particular. Details of the Taylor test will be given in section four below.

Over the last two decades, several models have been proposed for predicting hardening in large deformation plasticity. Three of these, Johnson-Cook[1] (JC), Steinberg-Cochran-Guinan[2] (SCG), and Mechanical Threshold Stress (MTS)[3] have been included in the current evaluation. The authors do not imply that these models have been presented by their respective developers without validating data, merely that that validation alone is insufficient to fairly compare one model to another. One reason for this is that the validating predictions presented in support of a given model was not necessarily arrived at through exactly the same numerical methods as that presented for another model. An unavoidable consequence of this is that any comparison of the predictive capabilities of these models that is based on the current literature alone will be, to some degree, an "apples-to-oranges" comparison. The present work is devoted to obtaining an "apples-to-apples" comparison by implementing all models to be evaluated in the same continuum code and then conducting a comparison wherein all factors other than the hardening model are kept identical. The decision to conduct all analyses in a

common code is important, for it is only by taking such an approach that we have any hope of evaluating subtle model differences.

The focus of this paper will be primarily on the framework within which these evaluations are being conducted, although some preliminary results will be presented. In the following, the code into which the above mentioned models have been implemented for the purpose of this work is described. The formulation of large deformation plasticity, of which the hardening model is a constituent part, will then be outlined. The formulation will be seen to be semi-implicit, employing associative flow, anisotropic yield, and isotropic hardening. Each of the three models under evaluation here will be discussed in-turn and in some detail. Comparisons to experimental data derived from tests involving two different copper materials and tantalum will be presented.

2 THE CONTINUUM MECHANICS CODE

The continuum mechanics code that we have chosen to use for the current study is CHAD[4] (Computational Hydrodynamics for Advanced Design). CHAD is a three dimensional code which employs the finite volume method of arriving at finite difference approximations to the governing field equations. These governing equations: conservation of mass, conservation of linear momentum, and conservtion of energy, form a hyperbolic set which is solved implicitly. The governing equations take the form:

$$\frac{d}{dt}\int_V \rho \, dV + \int_S \left[\rho \left(u_i - v_i\right)\right] n_i \, dS = 0 \tag{1}$$

$$\begin{aligned}\frac{d}{dt}\int_V \rho u_i \, dV + \int_S \left[\rho u_i \left(u_j - v_j\right) n_j + \left(\frac{p}{a} + \sigma_T \, \frac{2}{3}\rho K\right) n_i\right] \, dS = \\ \int_S \left(s_{ji} + \tau_{L_{ji}} + \sigma_T \tau_{T_{ji}}\right) n_j \, dS\end{aligned} \tag{2}$$

$$\begin{aligned}\frac{d}{dt}\int_V \rho h \, dV + \int_S \left[\rho h \left(u_i - v_i\right)\right] n_i \, dS = \\ \int_V \left(\frac{\partial p}{\partial t} + u_i p_{,i}\right) \, dV + \int_V \left(s_{ji} u_{i,j} + \tau_{ji} u_{i,j} + \sigma_T \rho \epsilon\right) \, dV - \int_S \left(q_{L_i} + \sigma_T q_{T_i}\right) \, dS\end{aligned} \tag{3}$$

Since the governing equations are written in rate form, we must must solve them in an incremental fashion marching through time. All tensors in the above are Eulerian. With the exception of Eq. (47), indicial notation applies throughout the paper. The variable u_i denotes the instantaneous velocity of a material point in the mathematical domain of interest and v_i denotes mesh velocity. Note that in this formulation advection is embedded into the governing equations. This obviates the two step (Lagrangian/remap) process that is standard in the classical ALE approach. Note also that the governing equations given above are in keeping with the assumption that the Cauchy stress, T_{ji}, takes the following form:

$$T_{ji} = s_{ji} + \tau_{ji} - p\delta_{ji} \tag{4}$$

where s_{ji} denotes the deviatoric stress, τ_{ji} denotes the viscous stress, p denotes the hydrostatic (or spherical) part of the stress tensor, and δ_{ij} is the Kroneker delta. It is noted that Eq. (4) is an unconventional interpretation of the Cauchy stress and may be in conflict with an interpretation founded on the experimental measurement of stress. It

is convenient, however, to think of the Cauchy stress in terms of such a notional tensor. This viewpoint facilitates the modeling of domains which exhibit both solid and fluid behaviors. Making the assumption that the Cauchy stress takes the notional form given in Eq. (4), we can derive Eqs. (1)-(3) from first principles and avoid adding terms such as artificial viscosity in an *ad hoc* manner. Whether we arrive at Eqs. (1)-(3) through the assumption of Eq. (4), or through some other manner, we must ultimately arrive at conservation of linear momentum and energy which includes both s_{ji} and τ_{ji} if we are to be able to handle both fluid and solid behaviors in an efficient manner. CHAD is written to handle the full range of solid-fluid behavior. Turbulence is incorporated thrugh the use of a K-ϵ model, with σ_T being a switch (1 if the flow is turbulent, 0 otherwise). Term σ_T was set to zero in the present work. Other variables appearing above include the density ρ, a unit outer normal n_i, the specific enthalpy h, the thermal flux q_i, and a pressure gradient scaling parameter, a. The pressure gradient scaling parameter can be used to improve computational efficiency for low mach number flows by giving it a value greater than one (it was set to unity in the current work). CHAD includes three additional sets of governing equations which are not explicitly addressed here. These are equations for calculating the species mass transport for chemically reactive flows, and for determining the turbulent kinetic energy K and its dissipation rate ϵ (necessary when $\sigma_T = 1$). Note that if the term s_{ij} were missing from the above, CHAD would be an advanced computational fluid dynamics code (one incorporating a turbulence model and advection). With s_{ij}, the code possesses an ability to predict the behavior of flowing solids as well as fluids. As discussed in O'Rourke and Sahota,[4] CHAD can be executed in Lagrangian mode, Eulerian mode, or something in-between. The analysis conducted herein was performed in a pure Lagrange mode.

3 THE PLASTICITY THEORY

Inspection of the governing field equations (just presented) reveals that the deviatoric stress tensor, s_{ij}, appears in conservation of linear momentum and in conservation of energy. In order to satisfy the governing field equations, it is therefore necessary to update the deviatoric stress on each time step. It is within the framework of classical plasticity that this is accomplished. In this section we delineate the method that has been adopted. It is based on a formulation presented by Maudlin and Schiferl.[5] We shall not develop that formulation here, but will present only the information necessary to enable this work to stand comprehensibly. The reader is referred to Maudlin and Schiferl[5] for additional detail.

3.1 Kinematics of deformation

A fundamental challenge in large deformation elastic-plastic constitutive modeling is satisfying the requirements of constitutive modeling invarience and kinematic consistency. Two distinct approaches have appeared in the literature. One approach is to conduct the modeling in a frame of reference that is fixed with respect to the deformation process (a "laboratory" or "global" frame), and employ an objective stress rate. The other option is to conduct the constitutive modeling in an unrotated (or "material") frame that is related to the laboratory frame by an explicit rigid body rotation. It is this later approach that has been adopted in the present work, and consequently, is the only approach discussed herein. The interested reader is referred to Maudlin and Schiferl[5] for more information on alternate approaches. It is noted that the approach taken here is more costly computationally, but offers greater capability, such as in the

modeling of anisotropic flow.

In adopting the material frame modeling approach to acheiving invarience, all independent tensors must be rotated from the global to the material frame in order to conduct the consitutive modeling (updating of s_{ij}), and this must be done on each time step. Once the constitutive modeling is completed, the updated s_{ij} is rotated from the material to the global frame prior to proceeding to the next time step. It is obvious then that kinematic consistency requires an accurate method for updating the rotation tensor, R_{ij}.

A rate of rotation tensor, Ω_{ij}, can be defined[5] as follows:

$$\Omega_{ij} \equiv \dot{R}_{ik} R^T_{kj} \tag{5}$$

The rate of rotation is easily manipulated to provide an expression for $\dot{R}_{ji}$.

$$\dot{R}_{ij} = \Omega_{ik} R_{kj} \tag{6}$$

Applying a central difference approximation to this expression (Hughes and Winget[6]) provides the updated rotation which we seek:

$$R_{kj}(t + \Delta t) = \left[\delta_{ik} - \frac{\Delta t}{2}\,\Omega_{ik}\right]^{-1} \left[\delta_{ik} - \frac{\Delta t}{2}\,\Omega_{ik}\right] R_{kj}(t) \tag{7}$$

Obviously for Eq. (7) to be applied, we require a means of determining Ω_{ij}. Dienes[7] has provided a straight-forward means of accomplishing this which gives Ω_{ij} in terms of the spin and left stretch tensors. It is easy to show that Ω_{ij} is antisymmetric. Consequently it can be expressed in terms of an axial vector, ω_i.

$$\Omega_{ik} = \varepsilon_{ijk}\omega_j \tag{8}$$

where ε_{ijk} is the Murnaghan (permutation) symbol. Following Dienes[7], the axial vector ω_i is calculated as follows:

$$\omega_i = w_i + [\delta_{il}\, V_{kk} - V_{il}]^{-1}\ z_l \tag{9}$$

where V_{ij} is the left stretch (Malvern[8]), w_i is the axial vector associated with the antisymmetric spin (or vorticity) tensor W_{ij} (Malvern[8]), and z_i is given as:

$$z_l = h_l V_{ii} - h_i V_{il} \tag{10}$$

where h_i is the axial vector associated with an antisymmetric tensor H_{ij}, defined as follows:

$$H_{pq} \equiv \Omega_{pq} - W_{pq} \tag{11}$$

One final kinematic detail must be addressed. Since Ω_{ij} is a function of the left stretch, it is obvious that this tensor too will have to be updated on each time step. To arrive at a relationship for updating the left stretch, we employ the polar decomposition theorem expressed in terms of the deformation gradient, F_{ij}, and the left stretch:

$$F_{ij} = V_{ik} R_{kj} \tag{12}$$

along with the relationship between the velocity gradient (Malvern[8]) and the deformation gradient:

$$L_{ij} = \dot{F}_{ik} F_{kj}^{-1} \tag{13}$$

Substituting (12) onto (13) yields the following relationship for the velocity gradient:

$$L_{ij} = \dot{V}_{il} V_{lj}^{-1} + V_{im} \Omega_{ml} V_{lj}^{-1} \tag{14}$$

Rearranging Eq. (14) so as to isolate $\dot{V}_{ij}$ and then applying a forward difference approximation yields the necessary update:

$$V_{ij}(t + \Delta t) = V_{ij}(t) + \left(L_{im} V_{mj} - V_{im} \Omega_{mj} \right) \Delta t \tag{15}$$

3.2 Updating the deviatoric stress

Classical plasticity consists of four parts: a stress-strain relation, a yield criterion, a hardening rule, and a flow rule, and it is classical plasticity that forms the basis for updating the deviatoric stress, s_{ij}.

The stress-strain relation, expressed in deviatoric rate form, is given as:

$$\begin{aligned} \dot{s}_{ij} &= 2\mu \eta_{ij}^{e} \\ &= 2\mu \left(\eta_{ij} - \eta_{ij}^{p} \right) \end{aligned} \tag{16}$$

where μ denotes the shear modulus and η_{ij} denotes the deviatoric part of the rate of deformation tensor[8] (deviatoric natural strain rate). Superscripts e and p are used to denote elastic and plastic parts, respectively. Note that all tensors appearing in this section reside in the material frame of reference. Implicit in the constitutive relation given above is the assumption that the elasticity is isotropic.

The anisotropic yield criterion is given as:

$$f = \frac{1}{2} \alpha_{ijkl} s_{ij} s_{kl} - \sigma^2 = 0 \tag{17}$$

where α_{ijkl} is a fourth order tensor of coefficients which defines the shape of the yield surface and σ is a flow stress which incorporates isotropic hardening and softening effects. Note that the yield surface is a function of deviatoric stress only and since $s_{kk} = 0$ this is a five dimensional space. Note also that this yield criterion accomodates von Mises J_2 plasticity, and Hill's quadratic criterion[9] (applicable to orthotropic media) as subsets. The hardening models will be discussed in the following section.

The associated flow rule (normality condition) is given as:

$$d_{ij}^{p} = \dot{\lambda} \frac{\partial f}{\partial s_{ij}} \tag{18}$$

where d_{ij} denotes the rate of deformation (natural strain rate) and $\dot{\lambda}$ is a time-dependent scalar. The fact that the normality condition is expressed in terms of the deviatoric

stress and not the total stress follows from the assumption that the yield surface is a function of deviatoric stress only.

As stated previously, our goal in this section is an update of the deviatoric stress. Following Nemat-Nasser,[10] this is accomplished by applying a finite difference approximation to a modified (but equivalent) form of Eq. (16). The term η_{ij}^{p}, appearing in Eq. (16) is calculated from the following:

$$\eta_{ij}^{p} = \dot{\gamma}\, u_{ij} \tag{19}$$

where

$$\dot{\gamma} \equiv \dot{\lambda}\sqrt{q_{ij}s_{ij}} \qquad u_{ij} \equiv \frac{q_{ij}}{\sqrt{q_{lm}s_{lm}}} \qquad q_{ij} \equiv \frac{\partial f}{\partial s_{ij}} \tag{20}$$

Substituting (19) into (16) produces:

$$\dot{s}_{ij} = 2\mu\left(\eta_{ij} - \dot{\gamma}\, u_{ij}\right) \tag{21}$$

and applying a forward difference approximation yields:

$$s_{ij}(t+\Delta t) = s_{ij}(t) + 2\mu\,\eta_{ij}\,\Delta t - 2\mu\,\Delta\gamma u_{ij} \tag{22}$$

Using previous time step values for all variables on the right-hand-side of Eq. (22) would represent an "explicit" solution. Nemat-Nasser[10] has provided a better-than-explicit, semi-implicit method. The essence of the method resides in: (1) the approximation of $\Delta\gamma$, and (2) using $(t+\Delta t)$ values of u_{ij}. It is through these two features that we achieve semi-implicitness. We shall discuss each of these features in turn.

The first step toward developing the semi-implicit character of $\Delta\gamma$ is to recast Eq. (21) into an analagous scalar form:

$$\dot{\tau} = \sqrt{2}\,\mu\,(d - c\dot{\gamma}) \tag{23}$$

where

$$\tau^2 \equiv \frac{1}{2}q_{ij}s_{ij} \qquad c \equiv u_{ij}u_{ij} \qquad d \equiv u_{ij}\eta_{ij} \tag{24}$$

Recognizing that $(d - c\dot{\gamma})$ represents the elastic part of the deviatoric part of the rate of deformation in this scalar constitutive equation, and making the assumption that all of the deviatoric part of the rate of deformation is plastic, implies the following:

$$\dot{\gamma} = \frac{d}{c} \tag{25}$$

In reality, most but not all of the deviatoric part of the rate of deformation will be plastic. We therefore modify Eq. (25) to take this into account by adding the error that would result from an assumption that the flow is completely plastic, $\dot{\gamma}_{er}$.

$$\dot{\gamma} = \frac{d}{c} - \dot{\gamma}_{er} \tag{26}$$

A forward difference approximation to Eq. (26) is given as:

$$\Delta\gamma = \frac{d}{c}\Delta t - \Delta\gamma_{er} \tag{27}$$

Using previous time step values for all variables on the right-hand-side of Eq. (27) would represent an "explicit" approximation of $\Delta\gamma$. We shall instead use a weighted average for d, thereby arriving at the better-than-explicit representation for $\Delta\gamma$ that we seek. We use previous time step values of c. If we use a superscript $*$ to denote a weighted average and a superscript $+$ to denote a previous time step value, we seek $\Delta\gamma$ such that:

$$\Delta\gamma = \frac{d^*}{c^+}\Delta t - \Delta\gamma_{er} \tag{28}$$

Hence our task now boils down to developing a suitable approximation for d^* and $\Delta\gamma_{er}$. Considering $\Delta\gamma_{er}$ first, if we substitute Eq. (28) into a forward difference approximation of Eq. (23), a little manipulation yields:

$$\Delta\gamma_{er} = \frac{\sqrt{2}\,\sigma(t+\Delta t) - \sqrt{q_{lm}\,s_{lm}}(t)}{2\,\mu\,c^+} \tag{29}$$

Finally, the weighted average for d is given as:

$$d^* = \left[u_{ij}^{\eta}\,\eta_{ij} + \frac{1}{2}\theta\left(u_{ij}^{q}\,\eta_{ij} - u_{ij}^{\eta}\,\eta_{ij}\right)\right]\sqrt{c^+} \tag{30}$$

where

$$u_{ij}^{\eta} = \frac{\eta_{ij}}{\sqrt{\eta_{lm}\,\eta_{lm}}} \qquad u_{ij}^{q} = \frac{q_{ij}}{\sqrt{q_{lm}\,q_{lm}}} \qquad \theta = \frac{d^* - c^+\dot{\gamma}^+}{d^*} \tag{31}$$

The term u_{ij}^{η} indicates the direction of deviatoric strain, the term u_{ij}^{q} indicates the direction of deviatoric plastic strain, and θ is a weighting function that represents the fraction of Δt that realizes elastic deformation. Note that d^* is a function of θ, and θ is a function of d^*, consequently, iteration is required to arrive at the weighted d^*.

We now have a formulation for the term $\Delta\gamma$ which possesses semi-implicitness. This term goes into Eq. (22) prior to solving for $s_{ij}(t+\Delta t)$. The remaining aspect of the method which imparts semi-implicitness is, as mentioned previously, in using $(t+\Delta t)$ values of the term u_{ij} appearing in Eq. (22). It is easy to show that $u_{ij}(t+\Delta t)$ can be written as a function of $s_{ij}(t+\Delta t)$. Consequently, we have $s_{ij}(t+\Delta t)$ on both the left and right hand sides of Eq. (22). Moving the right hand side terms to the left hand side and solving for $s_{ij}(t+\Delta t)$ imparts semi-implicitness to the solution.

3.3 The hardening models

The Johnson-Cook[1] model is a simple history independent model that depends on the current state of the equivalent plastic strain, equivalent plastic strain rate, and temperature. The model is given as:

$$\sigma = \left[\sigma_o + B\left(\epsilon^p\right)^n\right]\left[1 + C\,\ln\left(\dot{\epsilon}^p\right)\right]\left[1 - \left(\frac{T - T_r}{T_m - T_r}\right)^m\right] \tag{32}$$

where ϵ^p denotes the equivalent plastic strain, $\dot{\epsilon}^p$ denotes the equivalent plastic strain rate, σ_o denotes the initial yield, B is a strain hardening coefficient, n is a strain hardening exponent, C is a strain rate hardening coefficient, T_r denotes room temperature, T_m denotes melt temperature, and m is a softening exponent. Hence the first bracketed term in Eq. (32) represents strain hardening, the second strain rate hardening, and the third thermal softening. This model has seven input parameters: σ_o, B, n, C, T_r, T_m, and m. The equivalent plastic strain rate and equivalent plastic strain are determined as follows:

$$\dot{\epsilon}^p = \sqrt{\frac{2}{3}\eta_{ij}\eta_{ij}} \tag{33}$$

$$\epsilon^p(t+\Delta t) = \epsilon^p(t) + \int_t^{t+\Delta t} \dot{\epsilon}^p \, dt \tag{34}$$

The Steinberg-Cochran-Guinan[2] model, like Johnson-Cook, is a simple history independent model. It includes a method for adjusting the shear modulus as well as the flow stress and includes a melt criterion but has no explicit strain-rate dependence. Its developers claim that the model is expected to work so long as the strain rate is greater than about 10^5 s^{-1}. The model is given as:

$$\mu = \mu_0 \left\{ 1 + A\frac{p}{\eta^{1/3}} - B(T-300) \right\} \tag{35}$$

$$\sigma = \sigma_0 \left\{1+\beta(\epsilon^p+\epsilon_i)\right\}^n \left\{ 1 + A\frac{p}{\eta^{1/3}} - B(T-300) \right\} \tag{36}$$

$$A = \frac{1}{\mu_0}\frac{d\mu}{dP} \qquad B = \frac{1}{\mu_0}\frac{d\mu}{dT} \qquad \sigma_0 \left\{1+\beta(\epsilon^p+\epsilon_i)\right\}^n \leq Y_{\max} \tag{37}$$

$$T_m = T_{m0} \exp\left\{2a(1-1/\eta)\right\} \eta^{2(\Gamma_0 - a - 1/3)} \tag{38}$$

where p is the pressure, T is the temperature, μ_0 is the shear modulus at the reference state (T=300 K, p=0, ϵ^p=0), η is the compression (ρ/ρ_0), σ_0 is the reference state uniaxial yield strength, ϵ_i is the initial equivalent plastic strain, n and β are work hardening parameters, $Y_{\max}$ is the maximum value of uniaxial yield (at T=300 K and p=0) that can be found in the literature, T_{m0} is the melt temperature (at $\rho = \rho_0$), a is the coefficient of first-order volume correction to Grüneisen's gamma, and Γ_0 is the reference state value of Grüneisen's gamma. This model requires twelve input parameters: μ_0, σ_0, A, B, β, ϵ_i, $Y_{\max}$, n, a, Γ_0, T_{m0}, and ρ_0.

The MTS[3] model attempts to take history into account. It is phenomenological yet is based on dislocation mechanics in the sense that it attempts to macroscopically model contributions to the flow stress from dislocation interactions with barriers such as other dislocations, interstitial and solute atoms. Each of these interaction contributions is quantified through an internal state variable $\hat{\sigma}_i$ (i denotes interaction number). And each of these internal state variables has its own evolution law. The internal state variables which take into account structure evolution are coupled with constant-structure terms, S_i, (i denotes interaction number) that are primarily functions of strain rate and temperature. The model includes a term, $\hat{\sigma}_a$, called the athermal threshold stress which

represents dislocation interactions with long range barriers such as grain boundaries. This term is usually assumed to be constant. The model is given as follows:

$$\mu = b_1 - \frac{b_2}{\left(e^{\frac{b_3}{T}} - 1\right)} \tag{39}$$

$$\widehat{\sigma}_s = \widehat{\sigma}_{s0} \left(\frac{\dot{\epsilon}^p}{\dot{\epsilon}_{s0}}\right)^{\frac{kT}{\mu A b^3}} \tag{40}$$

$$X_i = \frac{\widehat{\sigma}_i}{\widehat{\sigma}_s} \qquad F(X_i) = \frac{\tanh(\alpha X_i)}{\tanh \alpha} \tag{41}$$

$$\theta_0 = a_0 + a_1 \ln \dot{\epsilon} + a_2 \sqrt{\dot{\epsilon}} \tag{42}$$

$$\frac{\partial \widehat{\sigma}_i}{\partial \epsilon} = \theta_0 [1 - F(X_i)] \qquad \Rightarrow \qquad \widehat{\sigma}_i(n+1) = \widehat{\sigma}_i(n) + \Delta\epsilon^p \, \theta_0 [1 - F(X_i)] \tag{43}$$

$$S_i = \left[1 - \left(\frac{kT \ln \frac{\dot{\epsilon}_i}{\dot{\epsilon}^p}}{\mu b^3 g_i}\right)^{\frac{1}{q_i}}\right]^{\frac{1}{p_i}} \tag{44}$$

$$\sigma = \widehat{\sigma}_a + \left(\frac{\mu}{\mu_0}\right) \sum_{i=1}^{N} \widehat{\sigma}_i \, S_i \tag{45}$$

where b_1, b_2, and b_3 are constants in the model for the shear modulus, a_0, a_1, and a_2 are constants in the hardening function θ_0, $\widehat{\sigma}_{s0}$ is the saturation stress at 0K, $\dot{\epsilon}_{s0}$ is the saturation stress reference equivalent plastic strain rate, A is a saturation stress fitting constant, k is Boltzmann's constant, b is Burger's vector, g_i is the normalized activation energy for interaction i, q_i and p_i are free energy exponents for interaction i, and α is a parameter normally set to 2. This model requires thirteen plus 5N input parameters (N being the number of relevant interactions): N, $\widehat{\sigma}_a$, $\dot{\epsilon}_i$, g_i, p_i, q_i, $\widehat{\sigma}_{i_0}$, b_0, b_1, b_2, $\widehat{\sigma}_{s0}$, $\dot{\epsilon}_{s0}$, A, b, a_0, a_1, a_2, α. Note that for most materials only one of the internal state variables ($\widehat{\sigma}_i$) actually evolves with time (the one related to dislocation-dislocation interaction), the remaining remain fixed at the given initial value. This is the case with the tantalum model to be presented below.

4 EXPERIMENTS AND COMPARISON TO PREDICTION

The Taylor cylinder impact test conducted to support the present work is depicted in Fig. 1. It is conceptually quite simple, involving the impact of a right circular cylinder onto the hardened surface of a massive anvil. The surface of the anvil is polished to a mirror finish so as to minimize friction between the anvil and impacting cylinder. Care is taken to align the gun so that the cylinder impacts with its axis normal to the hardened surface. The gun used in the present work is a 30 caliber smooth-bore gas gun with a peak pressure capability of about 13.79 MPa. This pressure will propel a copper cylinder at about 200 m/s.

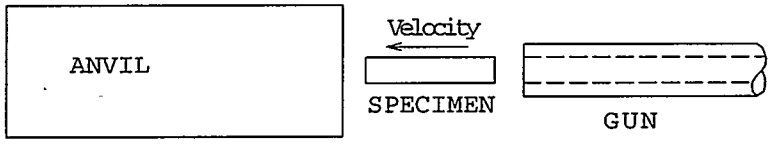

Figure 1. Taylor cylinder test

The objective in the present work was to conduct tests involving several different materials, and use the results of these tests to evaluate the ability of the continuum code with the plasticity described previously to predict the final deformed shape of the cylinder. In particular, we sought to use the results to evaluate the hardening models keeping all other aspects of the prediction equivalent. As mentioned previously, the Taylor test is considered a good test for the evaluation of plasticity models because it produces a wide range in material behaviors which serve to excercise many aspects of the model. For example, some materials respond to the impact in such a way that the plastic wave sweeps the entire length of the cylinder, while in other materials the plastic wave sweeps through only a fraction of the cylinder length. Some materials flow isotropically producing a circular footprint (the shape of the cylinder impact surface post-test), while other materials flow anisotropically producing a footprint that is non-circular (in many cases roughly elliptical). The development of a general model capable of capturing all of these responses makes for an interesting problem.

This work is, at the present time, in a preliminary stage. Included herein are the results of tests involving a fully annealed copper (specimens initially 2.54 cm in length, and 5.08 cm in length), a half-hardened copper (specimens initially 5.08 cm in length), and a tantalum material which exhibits significant anisotropy (specimens initially 3.81 cm in length). The impact velocity of the 2.54 cm annealed copper cylinder was 146 m/s, of the 5.08 cm annealed copper cylinder and of the half-hardened copper cylinder was 177 m/s, and of the tantalum cylinder was 175 m/s.

The hardening model parameters used in the analysis are presented in Tables 1-5. The data in Table 1 was obtained from Johnson and Holmquist,[11] the data in Table 2 was obtained from Steinberg,[12] and the data in Tables 3-5 was developed at Los Alamos National Laboratory by the third author and his colleagues. In general, the data for hardening models is obtained from uniaxial quasistatic and Hopkinson bar data. The elastic shear modulus (value of μ used in the calculation of the deviatoric stress while inside the yield surface) was 45.45 GPa for both copper materials and 75.39 GPa for Tantalum. The pressure was in all cases calculated using a Mie-Grüneisen equation of state of the form:

$$p = \frac{\rho_0 C_0^2 \zeta \left[1 + \left(1 - \frac{\Gamma_0}{2}\right)\zeta\right]}{\left[1 - (S_\alpha - 1)\zeta\right]^2} + \Gamma_0 E \tag{46}$$

where C_0 is the bulk sound speed, S_α is a linear Hugoniot slope coefficient, ζ is a measure of compression $(\frac{\rho}{\rho_0} - 1)$, and E is the internal energy. Bulk sound speed values used in the analysis were 3940 m/s for the copper materials and 3310 m/s for the tantalum. The parameter S_α was given the value 1.489 for the copper materials and 1.2 for the tantalum. The internal energy was calculated as the product of specific heat and temperature. Values of specific heat used in the analysis were 383 (Pa m^3)/(kg K) for the copper materilals and 135 (Pa m^3)/(kg K) for the tantalum. The failure surface shape parameters used in the analysis [α_{ijkl} of Eq. (17)] are given in Voigt-Mandel notation as follows:

$$[\alpha]^{V-M} = \begin{bmatrix} 2. & -1. & -1. & 0. & 0. & 0. \\ -1. & 2. & -1. & 0. & 0. & 0. \\ -1. & -1. & 2. & 0. & 0. & 0. \\ 0. & 0. & 0. & 2(1.5) & 0. & 0. \\ 0. & 0. & 0. & 0. & 2(1.5) & 0. \\ 0. & 0. & 0. & 0. & 0. & 2(1.5) \end{bmatrix} \quad \text{for copper}$$

$$= \begin{bmatrix} 2.522 & -1.3584 & -1.164 & 0. & 0. & 0. \\ -1.3584 & 2.195 & -0.8363 & 0. & 0. & 0. \\ -1.164 & -0.8363 & 2.0 & 0. & 0. & 0. \\ 0. & 0. & 0. & 2(1.791) & 0. & 0. \\ 0. & 0. & 0. & 0. & 2(2.582) & 0. \\ 0. & 0. & 0. & 0. & 0. & 2(2.287) \end{bmatrix} \quad \text{for tantalum} \tag{47}$$

Parameter	Description	Value
σ_0	Initial uniaxial yield	89.6E06 Pa
B	Strain hardening coefficient	292.E06 Pa
C	Strain rate hardening coeff.	0.025
n	Strain hardening exponent	0.31
m	Thermal softening exponent	1.09
T_r	Room temperature	294 K
T_m	Melt temperature	1356 K

Table 1. JC parameters for annealed Cu

Parameter	Description	Value
ρ_0	Reference state density	8930 kg/m^3
μ_0	Ref. state shear modulus	47.7E09 Pa
σ_0	Ref. state uniaxial yield strength	0.120E09 Pa
A	Pressure hardening coefficient	2.83E-11 Pa^{-1}
B	Thermal softening coefficient	3.77E-04
β	Strain haradening coefficient	36
n	Strain hardening exponent	0.45
ϵ_i	Initial equivalent plastic strain	0.
Y_{max}	Largest reported value, uniaxial yield	0.64E09 Pa
Γ_0	Ref. state Grüneisen's gamma	2.02
a	Coeff. 1st order vol. corr. Grüneisen's gamma	1.5
T_{m0}	Melt temperature at $\eta = 1$	1790 K

Table 2. SCG parameters for annealed Cu

Parameter	Description	Value
N	Number of interactions	1
$\widehat{\sigma}_a$	Athermal threshold sress	40.E06 Pa
$\dot{\epsilon}_1$	Thermal activation const	1.E07 s^{-1}
g_1	Normalized actication energy	1.6
p_1	Free energy exponent	2/3
q_1	Free energy exponent	1
$\widehat{\sigma}_{1_0}$	Initial mechanical threshold stress	0.
b_1	Shear modulus const	45.78E09 Pa
b_2	Shear modulus const	3.0E09 Pa
b_3	Shear modulus const	180 K
a_0	Hardening function const	2390.E06 Pa
a_1	Hardening function const	12.E06 Pa
a_2	Hardening function const	1.696E06 Pa
$\widehat{\sigma}_{s0}$	Saturation stress at 0K	770.E06 Pa
$\dot{\epsilon}_{s0}$	Saturation stress ref strain rate	1.E07 s^{-1}
A	Saturation stress const	0.2625
b	Burger's vector	2.55E-10 m
α	Parameter in $F(X_i)$	2

Table 3. MTS parameters for annealed Cu

Parameter	Description	Value
N	Number of interactions	1
$\widehat{\sigma}_a$	Athermal threshold sress	40.E06 Pa
$\dot{\epsilon}_1$	Thermal activation const	1.E07 s^{-1}
g_1	Normalized actication energy	0.6
p_1	Free energy exponent	2/3
q_1	Free energy exponent	1
$\widehat{\sigma}_{1_0}$	Initial mechanical threshold stress	410.E06 Pa
b_1	Shear modulus const	45.78E09 Pa
b_2	Shear modulus const	3.0E09 Pa
b_3	Shear modulus const	180 K
a_0	Hardening function const	2390.E06 Pa
a_1	Hardening function const	12.E06 Pa
a_2	Hardening function const	1.696E06 Pa
$\widehat{\sigma}_{s0}$	Saturation stress at 0K	770.E06 Pa
$\dot{\epsilon}_{s0}$	Saturation stress ref strain rate	1.E07 s^{-1}
A	Saturation stress const	0.2625
b	Burger's vector	2.55E-10 m
α	Parameter in $F(X_i)$	2

Table 4. MTS parameters for half-hard Cu

Parameter	Description	Value
N	Number of interactions	2
$\widehat{\sigma}_a$	Athermal threshold sress	40.E06 Pa
$\dot{\epsilon}_1$	Thermal activation const (interaction 1: dislocation)	1.E07 s^{-1}
$\dot{\epsilon}_2$	Thermal activation const (interaction 2: interstitial)	1.E07 s^{-1}
g_1	Normalized activation energy (interaction 1: dislocation)	1.6
g_2	Normalized activation energy (interaction 2: interstitial)	0.1236
p_1	Free energy exponent (interaction 1: dislocation)	2/3
p_2	Free energy exponent (interaction 2: interstitial)	0.5
q_1	Free energy exponent (interaction 1: dislocation)	1
q_2	Free energy exponent (interaction 2: interstitial)	1.5
$\widehat{\sigma}_{1_0}$	Initial mechanical threshold stress (interaction 1: dislocation)	0. Pa
$\widehat{\sigma}_{2_0}$	Initial mechanical threshold stress (interaction 2: interstitial)	1203.E06 Pa
b_1	Shear modulus const	65.25E09 Pa
b_2	Shear modulus const	0.380E09 Pa
b_3	Shear modulus const	40 K
a_0	Hardening function const	2000.E06 Pa
a_1	Hardening function const	0.
a_2	Hardening function const	0.
$\widehat{\sigma}_{s0}$	Saturation stress at 0K	350.E06 Pa
$\dot{\epsilon}_{s0}$	Saturation stress ref. strain rate	1.E07 s^{-1}
A	Saturation stress const.	1.6
b	Burger's vector	2.863E-10 m
α	Parameter in $F(X_1)$	2.

Table 5. MTS parameters for Ta

Comparisons between predicted deformed shape and measured deformed shape are presented in Figs 2-5. In all cases the mesh silhouette depicts the predicted deformed shape while the dots represent the measured deformed shape. The prediction of the deformed shape of the copper cylinders using the MTS model and the measured deformed shape are practically indestinguishable (Fig. 2). Note that the plastic wave swept the entire length of the annealed cylinders whereas it swept through only about half the length of the half-hardened cylinder. The model was able to capture both behaviors. The result using the SCG model to predict the deformed shape of the annealed copper cylinders (Fig. 3) is very good. The only obvious error in the SCG prediction is in the final cylinder length, with the predicted length being slightly greater than the measure length. The JC model does a poorer job of predicting the shape of the copper cylinders (Fig. 4), though not all that bad qualitatively. The JC model has the overall shape about right but predicts a final length that is too great and predicts a larger footprint than what is observed. Figure 5 shows the comparison between prediction and observation for the tantalum cylinder, with the prediction obtained using the MTS model. Note that unlike the copper cylinders, which flowed isotropically, the tantalum cylinder exhibited significant orthotropic flow. What is shown in Fig. 5 may be thought of as a "front view", "side view", and footprint view. The agreement in Fig. 5 is considered to be quite good.

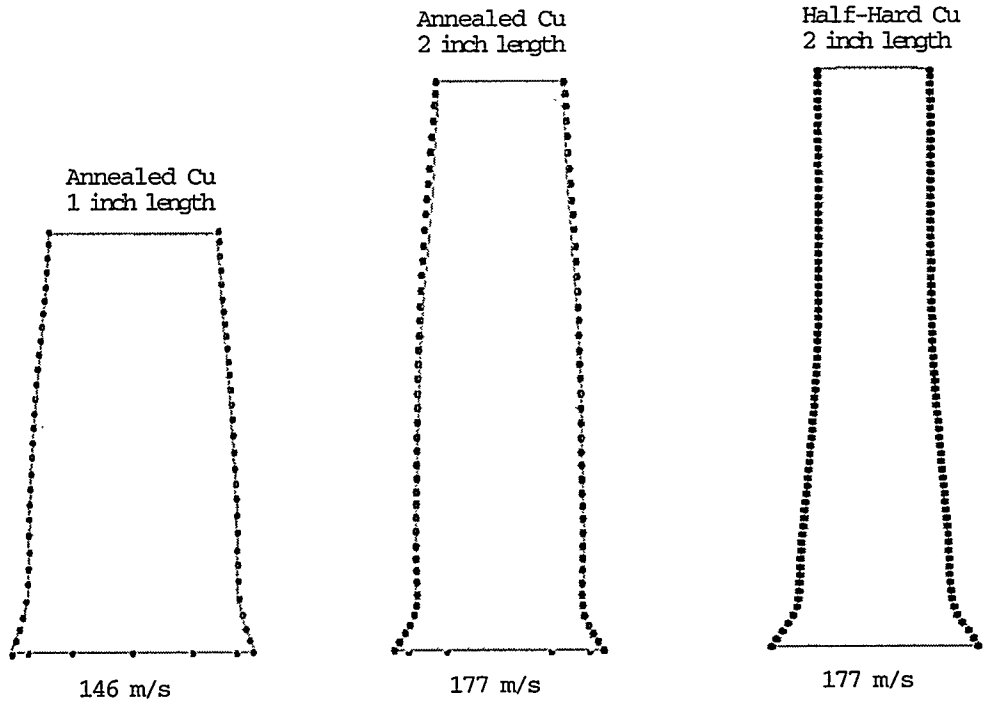

Figure 2. Copper cylinders, MTS hardening model

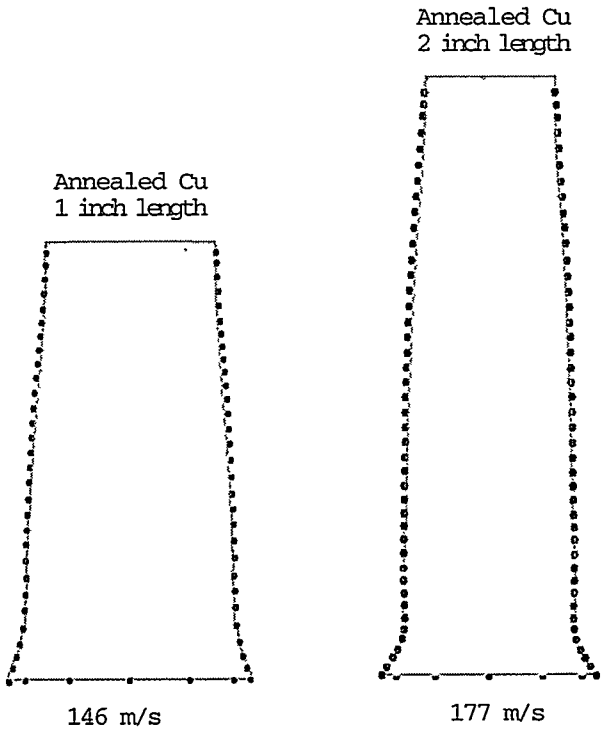

Figure 3. Copper cylinders, SCG hardening model

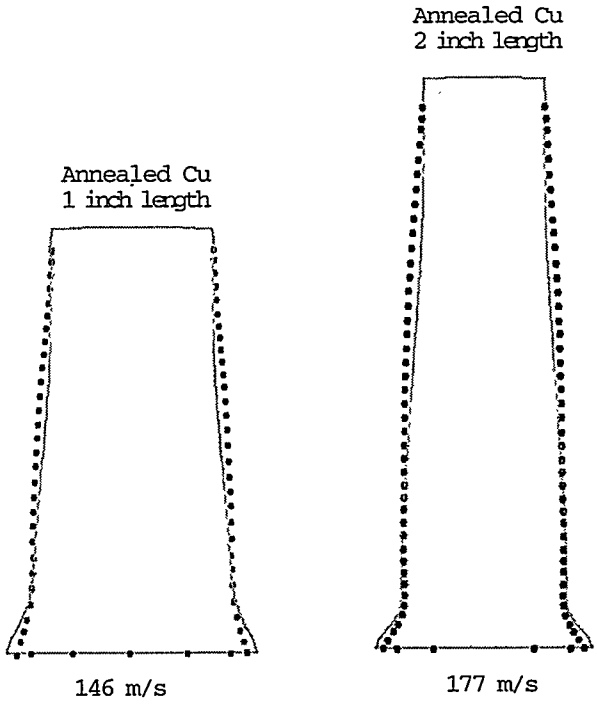

Figure 4. Copper cylinders, JC hardening model

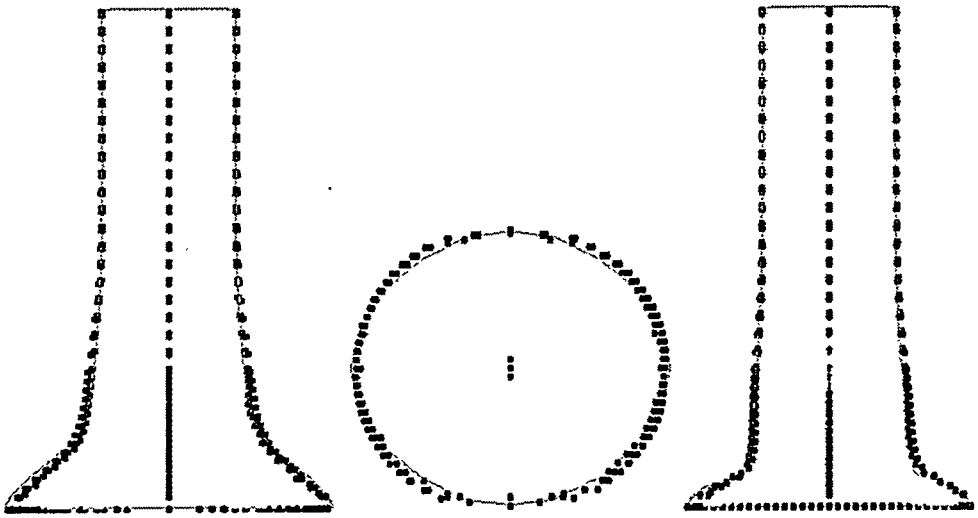

Figure 5. Tantalum cylinder, MTS hardening model

5 CONCLUSIONS

A framework for conducting a thorough "apples-to-apples" comparison of hardening models has been presented. This framework is based on an implementation of all models into the same continuum mechanics code and conducting the evaluation with all aspects of the analysis held constant, except for the hardening model. The hardening models exist as a constituent part of classical plasticity which is formulated in a semi-implicit numerical scheme that uses polar decomposition for kinematic consistency, associative flow for the evolution of plastic strain, and isotropic hardening for the evolution of the yield surface. The formulation is constructed so as to be able to handle anisotropic yield.

While the results presented here seem to indicate that the MTS model does the best job, followed by SCG and then JC, it is emphasized that this study is in a preliminary stage and firm conclusions require further work. The authors plan to present a more thorough evaluation when the data and analysis are available.

6 ACKNOWLEDGEMENTS

This work was performed under the auspices of the U.S. Department of Energy by Los Alamos National Laboratory under contract No. W-7405-ENG-36.

REFERENCES

[1] G.R. Johnson and W.H. Cook, "A Constitutive Model and Data for Metals Subjected to Large Strain, High Strain Rates, and High Temperatures," *Proceedings, 7th International Symposium on Ballistics*, The Hague, The Netherlands, 541-548 (1983).

[2] D.J. Steinberg, S.G. Cochran and M.W. Guinan, "A Constitutive Model for Metals Applicable to High-Strain Rate," *Journal of Applied Physics*, **51**, 1498-1504 (1980).

[3] P.S. Follansbee and U.F. Kocks, "A Constitutive Description of the Deformation of Copper Based on the use of the Mechanical Threshold Stress as an Internal State

Variable," *Acta Metallica*, **36**, 82-93 (1988).

[4] P.J. O'Rourke and M.S. Sahota, "A Variable Explicit/Implicit Numerical Method for Calculating Advection on Unstructured Meshes," *Journal of Computational Physics*, **143**, 312-345 (1998).

[5] P.J. Maudlin and S.K Schiferl, "Computational Anisotropic Plasticity for High-Rate Forming Applications," *Computer Methods in Applied Mechanics and Engineering*, **131**, 1-30 (1996).

[6] T.J.R. Hughes and J. Winget, "Finite Rotation Effects in Numerical Integration of Rate Constitutive Equations Arising in Large-Deformation Analysis," *International Journal for Numerical Methods in Engineering*, **15**, 1862-1867 (1980).

[7] J.K. Dienes, "On the Analysis of Rotation and Stress Rate in Deforming Bodies," *Acta Mechanica*, **32**, 217-232 (1979).

[8] L.E. Malvern, *Introduction to the Mechanics of a Continuous Medium*, Prentice-Hall, (1969).

[9] R. Hill, *The Mathematical Theory of Plasticity*, Oxford Press, London, Chapter 12, (1950).

[10] S. Nemat-Nasser, "Rate-Independent Finite-Deformation Elasto-Plasticity: A New Explicit Constitutive Algorithm," *Mechanics of Materials*, **11**, 235-249 (1991).

[11] G.R. Johnson and T.J. Holmquist, "Test Data and Computational Strength and Fracture Model Constants for 23 Materials Subjected to Large Strains, High Strain Rates, and High Temperatures," LA-11463-MS, Los Alamos National Laboratory, Los Alamos, NM (1989).

[12] D.J. Steinberg, "Equation of State and Strength Properties of Selected Materials," UCRL-MA-106439, Change 1, Lawrence Livermore National Laboratory, Livermore, CA (1996)